IEEE Access
Multidisciplinary ⋮ Rapid Review ⋮ Open Access Journal

Received 16 September 2023, accepted 2 October 2023, date of publication 5 October 2023, date of current version 11 October 2023.

Digital Object Identifier 10.1109/ACCESS.2023.3322364

RESEARCH ARTICLE

A Versatile 3-D Printable Model for Implementing Multiband Waveguide Filters With Flexible Filtering Characteristics

POVILAS VAITUKAITIS[1], (Graduate Student Member, IEEE), KENNETH NAI[2], AND JIASHENG HONG[1], (Fellow, IEEE)

[1]School of Engineering and Physical Sciences, Heriot-Watt University, EH14 4AS Edinburgh, U.K.
[2]Renishaw Plc, GL12 8JR Gloucester, U.K.

Corresponding author: Povilas Vaitukaitis (pv30@hw.ac.uk)

This work was supported in part by the Engineering and Physical Sciences Research Council (EPSRC), and in part by Renishaw Plc through the Industrial Cooperative Awards in Science and Technology (ICASE) Studentship (Voucher number 19000147) under Grant EP/T517471/1.

ABSTRACT This paper presents a novel multiband waveguide filter model employing cylindrical resonators arranged horizontally and vertically in Olympic and parallel topologies, respectively. The proposed model has the advantages of reduced footprint and the ability to realise more complex filtering functions. 3rd order dual-band, triple-band, quad-band and 5th order dual-band filters in *Ku*-band were designed to validate the proposed model. Design flexibility in terms of reconfigurability of centre frequencies and bandwidths is demonstrated with dual-band filter examples. The design strategy is presented and validated with a triple-band filter example. For experimental validation of the proposed model, Selective Laser Melting, a metal Additive Manufacturing technique, was used to fabricate triple-band filter prototypes in copper. Since this model has a complex internal structure, 3-D printing allowed us to avoid complicated assembly and manufacture filters in one piece. The measured results of the four prototypes show a good agreement with the simulations and adequate repeatability.

INDEX TERMS Dual-band filter, in-band transmission zeros, metal 3-D printing, multiband filter, parallel topology, quad-band filter, triple-band filter, waveguide filter.

I. INTRODUCTION

Multiband waveguide filters have found several uses in modern wireless communications systems. In systems operating in multiple separated frequency bands, multiband filters can reduce the number of components used, thus reducing footprint and cost [1]. Furthermore, in satellite communications, multiband waveguide filters can transmit several channels not contiguous in frequency through one beam, potentially using a single power amplifier, reducing power consumption and simplifying system architecture [1], [2].

The associate editor coordinating the review of this manuscript and approving it for publication was Photos Vryonides.

Generally, there are four ways to realise multiband filters [1]: via multimode resonators; combine single-band filters in parallel via manifold or circulators; cascading bandpass and bandstop filters; and utilise in-band transmission zeros (TZs) to separate one band into multiple. All four approaches can be realised in waveguide technology, albeit with various advantages and disadvantages. Waveguide filters are employed for high frequency applications, such as satellite communications since they have low loss and high power handling required to meet the specification.

Multimode resonators are a popular implementation for dual-band waveguide filters. Traditionally realised using cylindrical or elliptical cavities where it is possible to take advantage of orthogonally polarised degenerate modes with intrinsic isolation [3]. In [4] triple-band filter was realised

using three orthogonal modes in elliptical and rectangular cavities. Both implementations are very compact, retain a good measure of independent control of couplings, and have a high Q. However, this approach is limited to a maximum of three passbands and a wide guard-band, as even if the modes are orthogonal, they cannot be moved too close to each other without some interference.

The conventional manifold approach presents the best design flexibility for multiband waveguide filters. There is no limit to the number of bands and each band's specification can be controlled independently. The main drawbacks of this approach are the size, design complexity, as each channel has to be the same length, and it is impossible to have cross-couplings between nonadjacent resonators. Recently, a novel topology was proposed that alleviates some of the aforementioned drawbacks [5]. The folded topology allows to have cross-couplings and different channel lengths. However, the overall footprint is still relatively large compared to some of the other approaches.

Another implementation of parallel connected single-band waveguide filters was reported in [6]. Thin rectangular waveguide filters were stacked vertically and connected to input/output ports in parallel. Compared to the manifold approach, this reduced the footprint. However, there are some drawbacks to this implementation, namely, lower Q values (thin cavities), limit to the number of passbands, the higher the number of passbands, the thinner filters have to be, and some design flexibility is lost since it would be hard to realise different order passbands. Quad-band filter designed using this approach and simulated results were presented in [7].

Cascading a wide bandpass with a multi-notch filter presents a simple implementation of multiband waveguide filters, as each filter can be optimised separately. However, some challenges exist, such as realising a sharp rejection skirt over the guard-band and wide separation between channels [1], [4]. Also, the overall footprint is relatively large.

An in-band transmission zeros method has been utilised previously to design dual-band filters in combline resonator technology [8]. Dual-band and triple-band filter designs were demonstrated in substrate integrated waveguide (SIW) [9], microstrip [10], coaxial resonator [11], [12], and mixed waveguide and dielectric resonators [13] technologies. In waveguide technology, an in-band TZ approach has been reported in [14], [15], and [16]. However, [14] presented only simulation results, and [16] used an extended box topology that only applies to dual-band filters. All aforementioned waveguide implementations have narrow guard-band, which is one of the limiting factors of the in-band TZs method as wide frequency separation translates to large coupling values that cannot be realised physically [4].

This paper presents a novel, versatile implementation of an in-band transmission zeros approach in waveguide technology. The proposed waveguide model uses cylindrical resonators arranged in Olympic and parallel topologies, as shown in Fig. 1. Even though the same number of resonators are used to realise the same specification filters as in the manifold approach, the proposed model offers a smaller footprint. Olympic topology horizontally allows cross-coupling and reduces filter length, while parallel topology vertically further reduces footprint without diminishing Q value. Furthermore, a wide guard-band is possible due to the vertical coupling scheme's larger realisable coupling value. The intrinsic flexibility of the in-band TZs method in controlling the centre frequency and bandwidth and relatively low complexity of the physical implementation in terms of design parameters restrictions makes the proposed model versatile.

FIGURE 1. Proposed multiband waveguide filter implementation: cylindrical resonators arranged in Olympic (*z*-axis) and parallel (*y*-axis) topologies.

The physical structure of this model would be challenging to manufacture using traditional manufacturing techniques. Computer Numerical Control (CNC) milling would require filters to be manufactured in several parts, depending on the number of bands, and complicated assembly. Additive manufacturing (AM) has been successful in producing complex geometry filters [17], [18], [19], [20]. Therefore, metal 3-D printing, namely, Selective Laser Melting (SLM), was utilised to monolithically manufacture triple-band filter prototypes in copper.

This paper is organised as follows. Section II gives the proposed model's theoretical foundations, including detailed structure, coupling schemes, various multiband filter examples, and design strategy with a triple-band filter example. In Section III, manufacturing considerations, measured results of the four triple-band filter prototypes, and a discussion with a comparison of state-of-the-art multiband waveguide filter implementations are presented.

II. FILTER DESIGN

A. RESONATOR AND FILTER STRUCTURE

This multiband waveguide filter model uses cylindrical resonators arranged in Olympic topology in the *z*-axis and parallel topology in the *y*-axis, as shown in Fig. 1. Olympic topology allows to reduce filter length and introduce cross-coupling between non-adjacent resonators. Each row of resonators in the *y*-axis corresponds to a different passband, i.e., if there are two rows, as highlighted in Fig. 1, the filter will be dual-band. Consecutively, each column adds another pole to each passband.

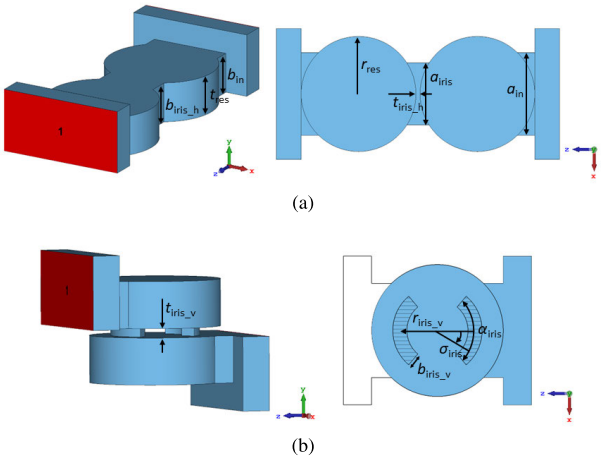

FIGURE 2. 3-D model with key dimensions of the coupling schemes: (a) horizontal; (b) vertical.

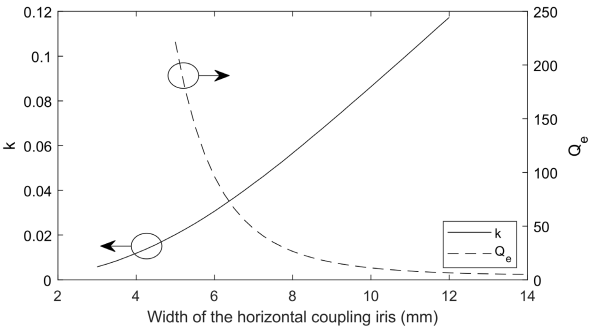

FIGURE 3. Coupling coefficient and external quality factor versus horizontal coupling iris width.

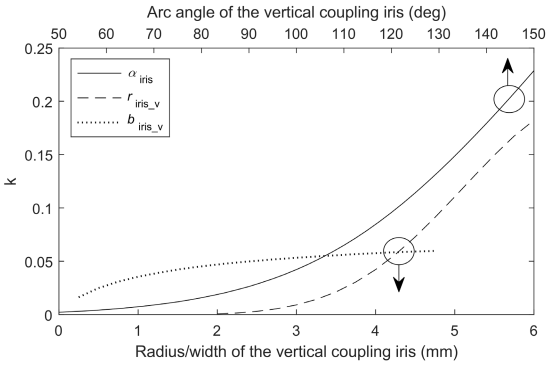

FIGURE 4. Coupling coefficient versus vertical coupling iris arc, radius, and width.

Key dimensions of the model are illustrated in Fig. 2. α_{iris} and σ_{iris} are the arc angle and angular position of the vertical coupling iris, respectively.

B. COUPLING OF RESONATORS

Two coupling schemes exist between resonators in this filter model. Horizontal coupling between resonators of the same row and vertical coupling between resonators of the same column, as illustrated in Fig. 2. Horizontal coupling is realised using the usual inductive iris, while vertical coupling

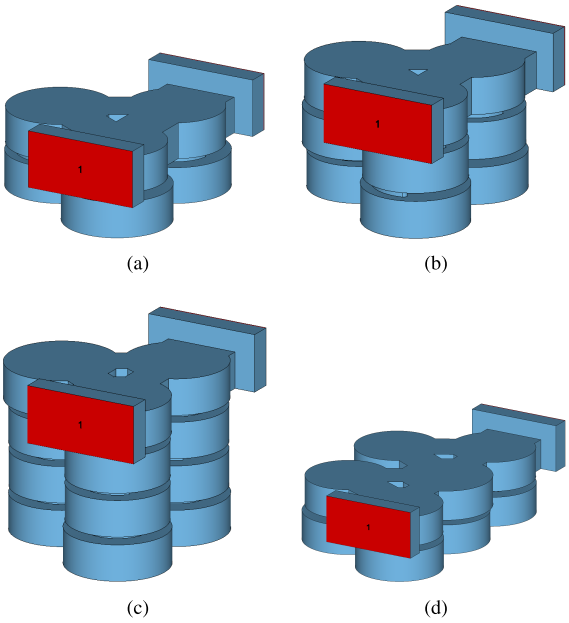

FIGURE 5. 3-D model of the: (a) 3rd order dual-band filter; (b) 3rd order triple-band filter; (c) 3rd order quad-band filter; (d) 5th order dual-band filter.

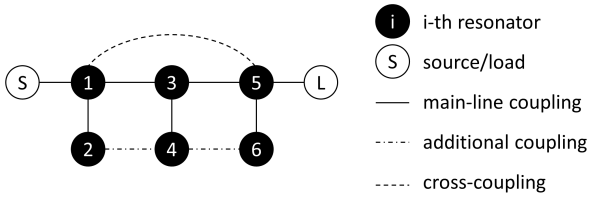

FIGURE 6. 3rd order dual-band filter topology.

is realised through two symmetrical arc irises. Two arc irises were used instead of one for symmetry reasons.

The main parameter to control coupling strength in horizontal coupling is the width of the iris. Meanwhile, for vertical coupling, the arc angle and radius of the coupling iris are the main parameters that control the coupling strength. The coupling coefficient and external quality factor versus respective parameters for horizontal and vertical coupling are shown in Figs. 3 and 4, respectively. Both coupling schemes have a wide range of coupling coefficients, which can be further increased using other parameters.

C. DUAL-BAND FILTER

Dual-band filter 3-D model and coupling topology are displayed in Figs. 5 and 6, respectively. If only main-line couplings are considered, the topology is the same as compound resonator multiband filters [1]. In this compound resonator coupling topology, it is possible to realise N transmission zeros in each guard-band, where N is the order of each passband. The TZs position is controlled solely via the resonance of shunt resonators (resonators in 2nd row in Fig. 6). Reflection poles are, as usual, controlled by all resonators.

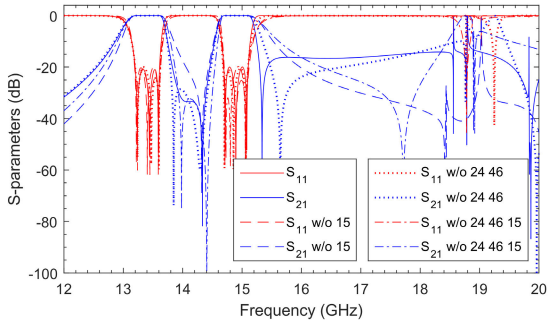

FIGURE 7. Simulated 3rd order dual-band filter frequency response for various coupling topologies (cf. Fig. 6). NB w/o 15 implies without coupling between 1st and 5th resonators, etc.

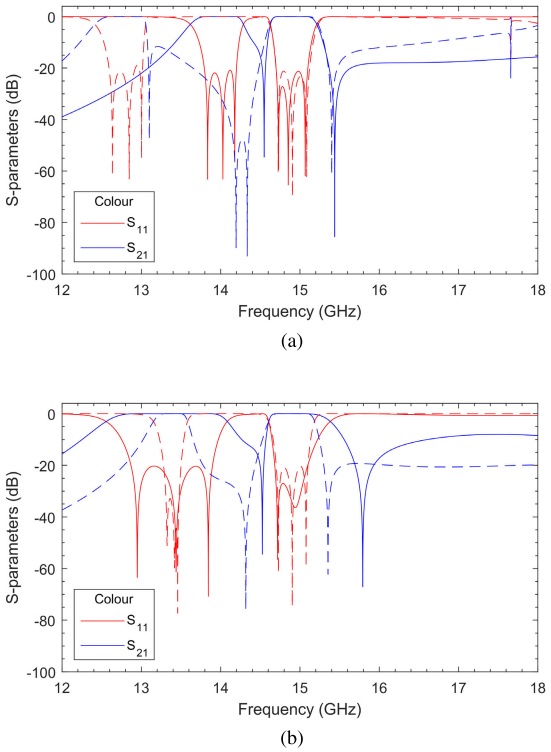

FIGURE 8. Simulated 3rd order dual-band filter frequency response showing reconfigurability of first passband's: (a) centre frequency while maintaining constant bandwidth and second passband; (b) bandwidth while maintaining constant centre frequency and second passband.

The simulated frequency response of the dual-band model for four cases of coupling topologies, with all couplings, without cross-coupling, without additional couplings, and without additional and cross-couplings, is shown in Fig. 7. Several conclusions can be drawn at this point. Cross-coupling happens even without the iris between the 1st and 5th resonators since the irises between the 1st and 3rd and 3rd and 5th resonators overlap. Thus created cross-coupling is weak, so TZ appears far in the stopband. In the case without additional couplings, there is higher rejection between the passbands but TZ above the second passband is further away. The reason why is this. With additional couplings, main-line couplings 13 and 35 are smaller; thus, irises are narrower,

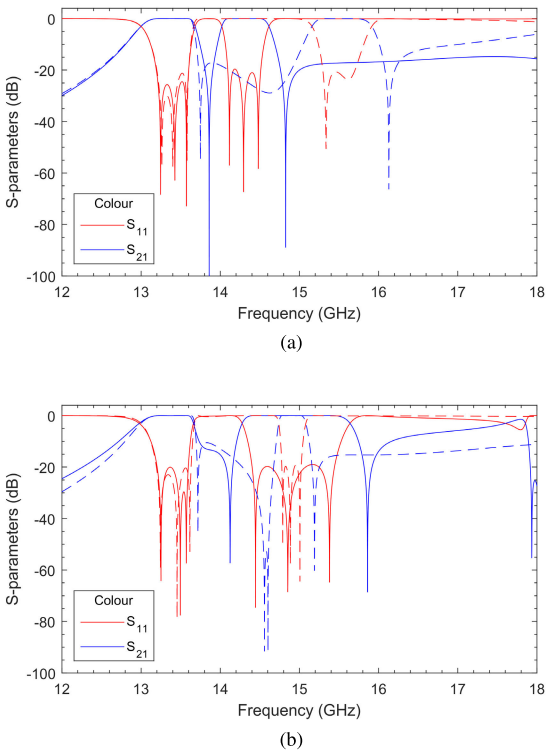

FIGURE 9. Simulated 3rd order dual-band filter frequency response showing reconfigurability of second passband's: (a) centre frequency while maintaining constant bandwidth and first passband; (b) bandwidth while maintaining constant centre frequency and first passband.

and in turn, the cross-coupling iris can realise the larger coupling required for TZ to be closer to the passband. For instance, in the filter without additional couplings, the irises widths were $a_{\text{iris13}} = 8.19$ mm and $a_{\text{iris15}} = 6.83$ mm, while in the filter with additional couplings, the irises widths were $a_{\text{iris13}} = 6.73$ mm and $a_{\text{iris15}} = 7.30$ mm. Additional couplings also might impact the realisable width of guard-band. Therefore, in this paper, all following filters were designed with additional and cross-couplings.

Since 3rd order dual-band filter is the simplest multiband filter of this model, it was used to demonstrate the design flexibility. Figs. 8 and 9 show the reconfigurability of the first and second passbands, respectively, in terms of centre frequency and bandwidth. This model can realise a wide range of centre frequency separations and bandwidths. However, there is a limit since spurious resonance is more excited and moves closer to the passbands when passband separation or bandwidths are large enough.

Due to how resonators are coupled in this model, it is impossible to have different order passbands.

D. DESIGN OF TRIPLE-BAND FILTER

A 3rd order triple-band filter with centre frequencies of 13.3/14.5/15.7 GHz and 400 MHz bandwidth for all channels will be designed to validate the design strategy. The same filter was manufactured as a prototype.

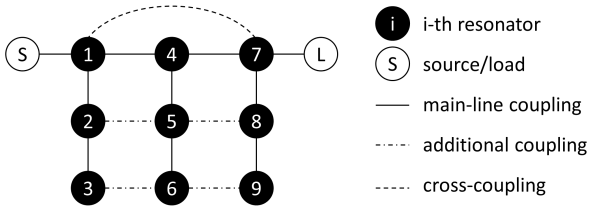

FIGURE 10. 3rd order triple-band filter topology.

The filter topology is illustrated in Fig. 10. To the best of the author's knowledge, there is no good way of synthesising the coupling matrix (CM) for such a topology. Therefore, a more straightforward approach was taken. When only main-line couplings are considered, the topology becomes the same as compound resonator multiband filters; thus, the transfer function and coupling matrix are easy to obtain. The transfer function was synthesised using the multi-prototype frequency transformation method [21]. From there, a folded coupling matrix can be obtained using the traditional methods. Then, the eigenvalue approach [22] was used to convert the folded coupling matrix to a coupling matrix of only the main-line coupling topology. The $N + 2$ coupling matrix is as shown at the bottom of the page in 1. It should be noted that similar CM could be obtained using an established reactance transformations method [23]. However, this technique has a couple of restrictions, such as the same order and return loss for all of the passbands; thus, the approach described above for determining CM was utilised in this work. The synthesised transfer function and coupling matrix responses are displayed in Fig. 11.

A few things about obtaining physical dimensions from the coupling matrix and Q_e and k graphs should be pointed out. In simulations to get said graphs, a simple structure is used, as shown in Fig. 2. This does not quite match with actual physical filter topology. For example, if coupling values are large between resonators in the same row, a physical dimension obtained from the k graph will also

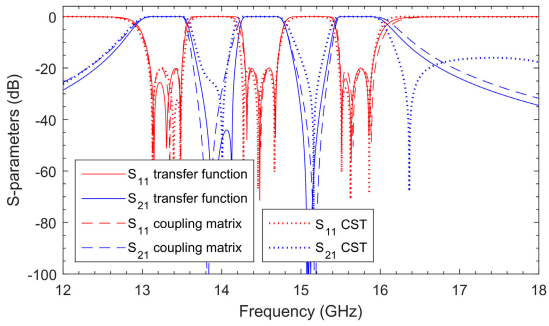

FIGURE 11. Synthesised transfer function, coupling matrix, and optimised simulated responses of 3rd order triple-band filter.

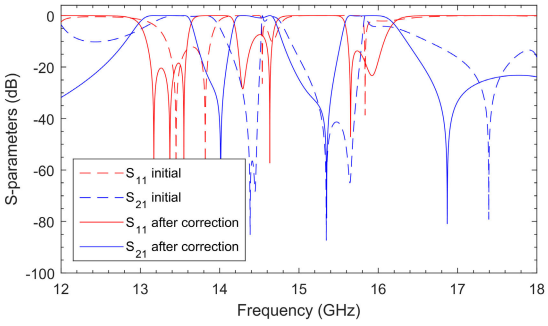

FIGURE 12. Simulated frequency response of 3rd order triple-band filter.

be large. However, due to cylindrical resonators arranged in Olympic topology, wide horizontal irises will overlap, as seen in Fig. 5b, irises between the 1st and 4th and 4th and 7th resonators overlap. Another consideration is the iris thickness, i.e. the distance between resonators. For example, the minimum wall thickness was set to 0.5 mm; therefore, the distance between the first and third columns of the second or higher rows of resonators is at a minimum of 0.5 mm. This means that the iris thickness is larger between smaller

$$\begin{bmatrix}
0 & 0.7282 & 0 & 0 & 0 & 0 & 0 & 0 & 0 & 0 & 0 \\
0.7282 & 0.0002 & 0.6689 & 0 & 0.4643 & 0 & 0 & 0 & 0 & 0 & 0 \\
0 & 0.6689 & -0.0080 & 0.4803 & 0 & 0 & 0 & 0 & 0 & 0 & 0 \\
0 & 0 & 0.4803 & -0.0678 & 0 & 0 & 0 & 0 & 0 & 0 & 0 \\
0 & 0.4643 & 0 & 0 & 0.0049 & 0.6686 & 0 & 0.4643 & 0 & 0 & 0 \\
0 & 0 & 0 & 0 & 0.6686 & -0.0099 & 0.4807 & 0 & 0 & 0 & 0 \\
0 & 0 & 0 & 0 & 0 & 0.4807 & -0.0704 & 0 & 0 & 0 & 0 \\
0 & 0 & 0 & 0 & 0.4643 & 0 & 0 & 0.0002 & 0.6689 & 0 & 0.7282 \\
0 & 0 & 0 & 0 & 0 & 0 & 0 & 0.6689 & -0.0080 & 0.4803 & 0 \\
0 & 0 & 0 & 0 & 0 & 0 & 0 & 0 & 0.4803 & -0.0678 & 0 \\
0 & 0 & 0 & 0 & 0 & 0 & 0 & 0.7282 & 0 & 0 & 0
\end{bmatrix} \quad (1)$$

TABLE 1. Main parameters of 3rd order triple-band filter design example.

Parameter	Value (mm)		Parameter	Value (deg)	
	Initial	After correction		Initial	After correction
a_{in}	10.38	10.38	α_{iris12}	123.2	123.2
a_{iris14}	9.96	7.5	α_{iris23}	118.08	118.08
a_{iris17}	0	5	α_{iris45}	123.1	123.1
a_{iris25}	0	5	α_{iris56}	118.1	118.1
a_{iris36}	0	5	σ_{iris12}	0	25
r_{res1}	6.99	6.99	σ_{iris23}	0	-25
r_{res2}	6.57	6.57	σ_{iris45}	0	25
r_{res3}	6.93	6.93	σ_{iris56}	0	-25
r_{res4}	6.72	6.72			
r_{res5}	6.57	6.57			
r_{res6}	6.94	6.94			

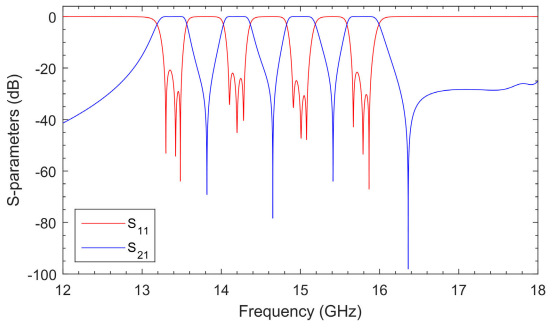

FIGURE 13. Simulated frequency response of 3rd order quad-band filter.

resonators, which needs to be accounted for as it affects the coupling strength.

The initial response obtained using the coupling matrix in 1 is shown in Fig. 12. This filter has no additional or cross-couplings. The first thing that needs to be adjusted is the horizontal iris width, a_{iris14} (and consecutively a_{iris47} as the filter is symmetrical), since both irises overlap. After that, additional and cross-couplings can be introduced and adjusted to obtain a better initial response. Finally, vertical irises were put into alternating positions to improve the stopband (see Appendix A). The response after these corrections is shown in Fig. 12. Such a response is a great starting point for optimisation and obtaining the final filter response as displayed in Fig. 11.

Table 1 shows the main parameters of the triple-band filter used to obtain initial and after correction responses. Other parameters were set to be the same for all resonators or irises and are as follows: $b_{in} = t_{res} = b_{iris\_h} = 5$ mm, $t_{iris\_v} = 1$ mm, $r_{iris\_v} = 4$ mm, $t_{iris\_h} = 0.5$ mm (between all columns), and $b_{iris\_v} = 1.5$ mm.

E. 5TH ORDER DUAL-BAND AND 3RD ORDER QUAD-BAND FILTERS

To further validate this model, another two filters, higher order dual-band and quad-band, were designed.

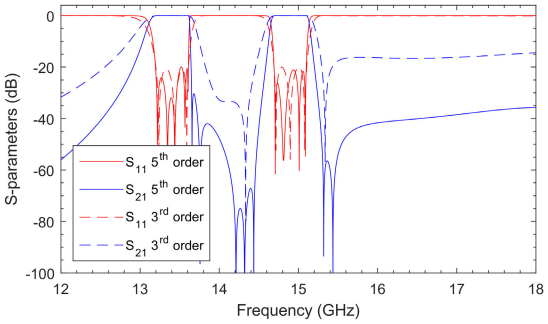

FIGURE 14. Simulated frequency response of 3rd and 5th order dual-band filters.

The 3rd order quad-band filter model and response are shown in Figs. 5c and 13, respectively. This filter was slightly more challenging to optimise than the triple-band filter. The main reason for this was lower design freedom due to the increased number of rows; as all resonators in a column are centred in respect to each other, there is only one iris thickness (t_{iris_h}) parameter between two columns. Thus, independently controlling all coupling coefficients and resonance frequencies is somewhat more complicated. More control could be achieved by introducing more design parameters. For example, off-centred resonators do not seem to excite any asymmetrical modes. Hence, each resonator could have up to two additional design parameters.

The 5th order dual-band filter model and response are shown in Figs. 5d and 14, respectively. The 5th order filter has better selectivity and higher rejection in the stopbands due to the higher filter order and increased number of TZs. The filter follows the same coupling scheme as the triple-band filter in Fig. 10, i.e. all adjacent resonators are coupled, and the only two cross-couplings are between the 1st and 5th and 5th and 9th resonators (following the same naming pattern as in Fig. 10). It should be noted that even order filters are possible to realise using this model.

III. EXPERIMENTAL RESULTS

To experimentally validate the proposed model, a 3rd order triple-band filter was manufactured using Selective Laser Melting. The four prototypes were fabricated using commercially pure copper (>99.5%) powder. The printed triple-band filter prototypes are shown in Fig. 15.

A. MANUFACTURING CONSIDERATIONS

The prototypes were printed at a 45° angle to avoid any overhangs. A smaller section of the metal shell between two resonators in a column is shown in Fig. 16. The angular position of vertical irises had to be restricted to parallel to the printing direction position to avoid overhangs. Also, the arc iris edges were blended to ensure further no overhangs when the irises are rotated within $\sigma_{iris} \in [-30, 30]$ interval. As with previous prototypes, most model edges were blended to avoid sudden changes in dimensions and thus improve printing quality.

TABLE 2. Comparison with state-of-the-art multiband waveguide filter implementations.

Ref.	Multiband Technology	Size	Design Complexity	Design Flexibility № of bands	Band order	f_0 and BW	Notes
[4], [24]	Multimode resonators	Small	High	Dep.	Dep.	Ind.	CM representation Limit to wide guard-band Limit to bandwidth <2% Max number of bands $\leq$3
[5]	Folded single-band filters with manifold	Large	High	Ind.	Ind.	Ind.	Channel length is not restricted Cross-coupling is possible
[6], [7]	Single-band filters in parallel	Medium	Medium	Dep.	Dep.	Ind.	Q decreases as channel number increases Each channel must be the same length
T.W.	In-band TZs	Medium	Medium	Ind.	Dep.	Ind.	CM representation Wide guard-band is possible Cross-coupling is possible

T.W. – this work; f_0 – centre frequency; BW – bandwidth; Dep. – dependent; Ind. – independent.

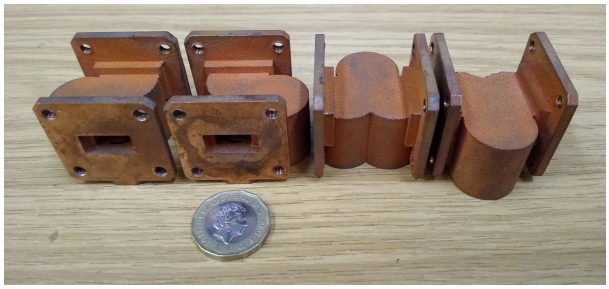

FIGURE 15. Photo of the four 3rd order triple-band filter prototypes fabricated using SLM (Renishaw RenAM 500Q machine).

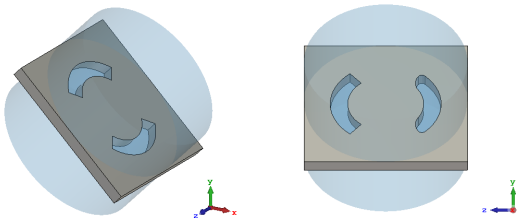

(a) (b)

FIGURE 16. Small section of metal shell around vertical coupling iris between two resonators in printing direction (*y*-axis): (a) perspective view when both irises are perpendicular to the printing direction; (b) front view when both irises are parallel to the printing direction.

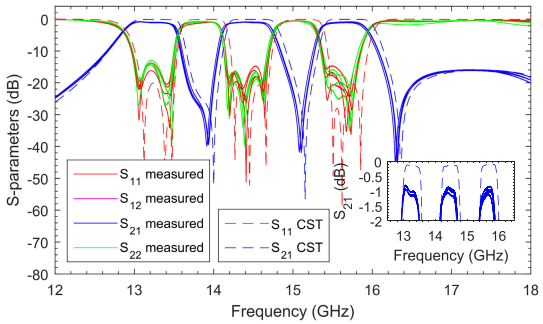

FIGURE 17. Four 3rd order triple-band filter prototypes' measured response (inset: insertion loss).

B. MEASURED RESULTS

The measured results of the four printed prototypes are shown in Fig. 17. The agreement with the simulated results is good. All prototypes showed a consistent response without any post-tuning. The simulated and measured insertion loss is about 0.15 dB and 1.1 dB at the centre frequency of each band, respectively. The measured in-band return loss is lower than 13 dB across all bands.

These prototypes were tested as-built without any post polishing. As shown previously, surface roughness could be significantly reduced by electro-polishing the prototypes, thus improving insertion loss [25]. Furthermore, as the measurement setup was identical to the one in [25], the test fixture included two coaxial to waveguide adapters which were not de-embedded. Thus, there are some additional losses.

C. DISCUSSION

Table 2 gives a comparison of state-of-the-art multiband waveguide filter implementations. Only waveguide filters capable of realising triple and higher-band filters were selected for this comparison. The comparison criteria include physical size, design complexity in filter synthesis and physical implementation, and design flexibility regarding the ability to control/realise the number of bands, individual band order, and centre frequency and bandwidth.

Multimode multiband waveguide filters have the smallest footprint of all possible implementations. This comes at the cost of high design complexity, as controlling input/output and inter-resonator couplings independently in triple-band filters is quite challenging. E.g., one of the three couplings is realised through an electrical probe, which complicates the physical structure and tuning of the filter [4]. Furthermore, there are other disadvantages, such as a limit to a wide guard-band and bandwidth due to stray couplings between modes and limited realisable coupling values, respectively.

Without a doubt, folded single-band filters with manifold present the most flexible implementation for multiband

waveguide filters [5]. The number of bands is unlimited, and each band's order, centre frequency, and bandwidth can be controlled independently. Also, cross-coupling is possible in folded topology, thus further improving filter response. The only downsides are high design complexity and large size. For example, each channel is first designed with in-line configuration, then folded without cross-coupling, then cross-coupling is introduced, then added to the manifold one by one, and then final optimisation can take place. At each step, some optimisation is required to maintain the desired response.

Single-band filters connected in parallel can be considered channel-dropping multiband filter implementation [6]. It works by designing a single-band filter with a wide stopband and then inserting further passbands within that stopband. The design process of each single-band filter is not very complicated; the only real restriction is that each channel has to be the same length. However, this does mean that different order bands are difficult/impossible to realise unless higher order modes are employed. Furthermore, the number of bands is restricted to the height of the input waveguide, and the Q value decreases as the number of bands increases.

In this work, an in-band TZs multiband waveguide filter implementation was presented. The proposed model incorporates cross-coupling and vertical stacking, allowing a wide guard-band to be realised. Even though it uses the same number of resonators to realise the same multiband filter as the manifold approach, the footprint is reduced as no manifold is needed and spacing between channels is eliminated. Furthermore, design complexity is relatively lower than multimode and manifold methods since multiband filter physical dimensions can be directly recovered from the coupling matrix, as demonstrated earlier. The hard part of the design is to synthesise the CM, but there are established methods for that [1], [14], [23].

IV. CONCLUSION

This article proposed a novel multiband waveguide filter topology. This topology offers a reduced footprint, the ability to realise advanced filtering functions, and excellent design flexibility. A triple-band filter was metal 3-D printed for experimental validation. The measured results had good agreement with the simulations.

In the future, higher-band filters could be designed to investigate whether there is a limit to how many bands this model can have. Also, filter topology without additional couplings should be investigated more thoroughly, as only a dual-band filter without additional couplings was designed.

APPENDIX A
SPURIOUS RESONANCE

Two factors determine the spurious-free window. The first is the resonator thickness, t_{res}. The thickness also affects the Q-factor, as shown in Fig. 18. $t_{res} = 5$ mm was chosen for all designed models in this paper as it offers maximum Q_u without reducing spurious-free window.

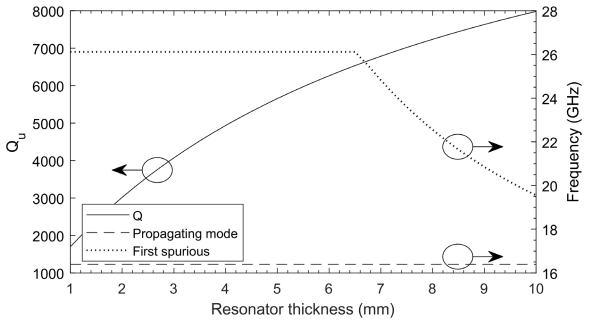

FIGURE 18. Cylindrical resonator, $r_{res} = 7$ mm, unloaded quality factor and first two modes frequency versus resonator thickness.

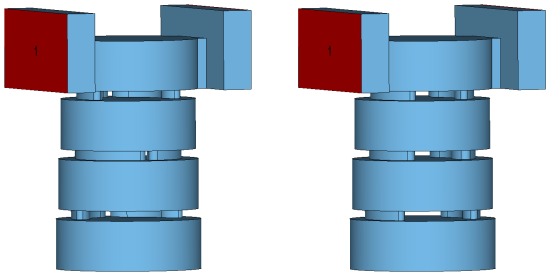

FIGURE 19. 3-D model of the 1st order quad-band filter with vertical irises in: (a) alternating angular position; (b) aligned angular position.

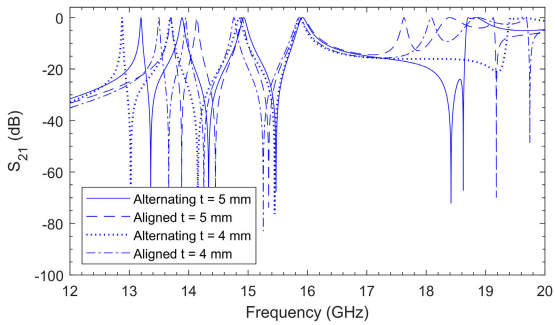

FIGURE 20. Simulated S_{21} response of the 1st order quad-band filter for various vertical irises angular positions and resonator thickness.

The second factor is not as obvious. The alignment of vertical coupling irises also affects the spurious resonance. The 3-D models of four resonators vertically coupled with two different cases of iris alignment are shown in Fig. 19. The corresponding responses are shown in Fig. 20. As can be seen, the spurious resonance is noticeably closer to the passbands when the vertical irises are aligned. Therefore, to improve the stopband, irises have to be alternated and/or resonator thickness has to be reduced.

It should be noted that although the angular position of vertical irises affects passband modes, this effect can be negated via other design parameters.

ACKNOWLEDGMENT

The authors would like to thank the staff at Renishaw Plc and the mechanical workshop at Heriot-Watt for their help manufacturing the prototypes.

REFERENCES

[1] R. J. Cameron, C. M. Kudsia, and R. R. Mansour, *Microwave Filters for Communication Systems: Fundamentals, Design, and Applications*. Hoboken, NJ, USA: Wiley, 2018.

[2] S. Holme, "Multiple passband filters for satellite applications," in *Proc. 20th AIAA Int. Commun. Satell. Syst. Conf. Exhib.*, May 2002, p. 1993.

[3] L. Zhu, R. R. Mansour, and M. Yu, "Compact waveguide dual-band filters and diplexers," *IEEE Trans. Microw. Theory Techn.*, vol. 65, no. 5, pp. 1525–1533, May 2017.

[4] L. Zhu, R. R. Mansour, and M. Yu, "Triple-band cavity bandpass filters," *IEEE Trans. Microw. Theory Techn.*, vol. 66, no. 9, pp. 4057–4069, Sep. 2018.

[5] J. C. Melgarejo, S. Cogollos, M. Guglielmi, and V. E. Boria, "A new family of multiband waveguide filters based on a folded topology," *IEEE Trans. Microw. Theory Techn.*, vol. 68, no. 7, pp. 2590–2600, Jul. 2020.

[6] Z.-C. Guo, G. Zhang, Y.-P. Lyu, and L. Zhu, "Multiband waveguide filters with compact size and large frequency ratio," *IEEE Trans. Plasma Sci.*, vol. 50, no. 3, pp. 761–766, Mar. 2022.

[7] Z.-C. Guo, L. Chen, and G. Zhang, "Design of a quad-band waveguide filter with compact size and large frequency ratio," in *IEEE MTT-S Int. Microw. Symp. Dig.*, vol. 1, Aug. 2022, pp. 1–3.

[8] G. Macchiarella and S. Tamiazzo, "Design techniques for dual-passband filters," *IEEE Trans. Microw. Theory Techn.*, vol. 53, no. 11, pp. 3265–3271, Nov. 2005.

[9] X.-P. Chen, K. Wu, and Z.-L. Li, "Dual-band and triple-band substrate integrated waveguide filters with Chebyshev and quasi-elliptic responses," *IEEE Trans. Microw. Theory Techn.*, vol. 55, no. 12, pp. 2569–2578, Dec. 2007.

[10] M. Mokhtaari, J. Bornemann, K. Rambabu, and S. Amari, "Coupling-matrix design of dual and triple passband filters," *IEEE Trans. Microw. Theory Techn.*, vol. 54, no. 11, pp. 3940–3946, Nov. 2006.

[11] K. Zhao and D. Psychogiou, "Monolithic multiband coaxial resonator-based bandpass filter using stereolithography apparatus (SLA) manufacturing," *IEEE Trans. Microw. Theory Techn.*, vol. 70, no. 9, pp. 4156–4166, Sep. 2022.

[12] K. Zhao and D. Psychogiou, "Vertically integrated coaxial resonator-based multiband bandpass filters using SLA 3-D printing," *IEEE Microw. Wireless Technol. Lett.*, vol. 33, no. 7, pp. 1–4, 2023.

[13] P. Boe, D. Miek, F. Kamrath, and M. Höft, "Dual-band filter composed of dielectric and waveguide resonators with in-band transmission zeros," in *IEEE MTT-S Int. Microw. Symp. Dig.*, Nov. 2021, pp. 73–75.

[14] P. Meyer and T. G. Brand, "Design equations for multi-band coupled-resonator filters using reactance mapping," in *Proc. Asia–Pacific Microw. Conf. (APMC)*, vol. 1, Dec. 2015, pp. 1–3.

[15] M. Guo, M. Lancaster, and C. Constantinou, "A new multi-passband filter synthesis technique," in *Proc. ARMMS Conf.*, 2015, pp. 1–15.

[16] S. Bila, R. Cameron, P. Lenoir, V. Lunot, and F. Seyfert, "Chebyshev synthesis for multi-band microwave filters," in *IEEE MTT-S Int. Microw. Symp. Dig.*, Jun. 2006, pp. 1221–1224.

[17] J. Rao, K. Nai, J. Marques-Hueso, P. Vaitukaitis, and J. Hong, "Inline quasi-elliptic bandpass filter based on metal 3-D printing technology," *IEEE Trans. Microw. Theory Techn.*, vol. 70, no. 4, pp. 2156–2164, Apr. 2022.

[18] Q. Liu, Y. Zhang, F. Zhang, and J. Xu, "A 3D printed waveguide hybrid bandpass filter integrated with twisting and bending functionalities," in *Proc. IEEE Int. Symp. Antennas Propag. USNC-URSI Radio Sci. Meeting (AP-S/URSI)*, Jul. 2022, pp. 2000–2001.

[19] C. Tomassoni, O. A. Peverini, G. Venanzoni, G. Addamo, F. Paonessa, and G. Virone, "3D printing of microwave and millimeter-wave filters: Additive manufacturing technologies applied in the development of high-performance filters with novel topologies," *IEEE Microw. Mag.*, vol. 21, no. 6, pp. 24–45, Jun. 2020.

[20] P. Vaitukaitis, K. Nai, J. Rao, and J. Hong, "On the development of metal 3D printed bandpass filter with wide stopband based on deformed elliptical cavity resonator with an additional plate," *IEEE Access*, vol. 10, pp. 15427–15435, 2022.

[21] X. Chen, "Synthesis of multi-band filters based on multi-prototype transformation," *IET Microw., Antennas Propag.*, vol. 15, no. 2, pp. 103–114, Feb. 2021.

[22] P. Kozakowski, A. Lamecki, P. Sypek, and M. Mrozowski, "Eigenvalue approach to synthesis of prototype filters with source/load coupling," *IEEE Microw. Wireless Compon. Lett.*, vol. 15, no. 2, pp. 98–100, Feb. 2005.

[23] T. G. Brand, P. Meyer, and R. H. Geschke, "Designing multiband coupled-resonator filters using reactance transformations," *Int. J. RF Microw. Comput.-Aided Eng.*, vol. 25, no. 1, pp. 81–92, Jan. 2015.

[24] L. Zhu, "High-Q multi-band filters," Ph.D. dissertation, Dept. Elect. Comput. Eng., Univ. Waterloo, Waterloo, ON, Canada, 2019.

[25] P. Vaitukaitis, K. Nai, J. Rao, M. S. Bakr, and J. Hong, "Technological investigation of metal 3-D printed microwave cavity filters based on different topologies and materials," *IEEE Trans. Compon., Packag., Manuf. Technol.*, vol. 12, no. 12, pp. 2027–2037, Dec. 2022.

POVILAS VAITUKAITIS (Graduate Student Member, IEEE) received the M.Eng. degree (Hons.) in mechanical engineering from the University of Aberdeen, Aberdeen, U.K., in 2019. He is currently pursuing the Ph.D. degree in electrical engineering with Heriot-Watt University, Edinburgh, U.K.

His current research interests include microwave passive device design and manufacturing using metal additive manufacturing technologies.

Mr. Vaitukaitis received the Project Award for an outstanding master's thesis project from the Institution of Mechanical Engineers (IMechE), in 2019.

KENNETH NAI received the B.Sc. degree (Hons.) in electronics and electrical engineering and the Ph.D. degree in control systems from Loughborough University, Loughborough, U.K., in 1990 and 1995, respectively.

He has been with Renishaw Plc, Wotton-Under-Edge, U.K., since 1995, where he is currently a Principal Engineer, and has developed products in the field of metrology systems, neurosurgical robotics, and metal powder 3-D printers. He is a Chartered Engineer and a member of the Institution of Engineering and Technology. He has been granted 11 U.S. patents.

JIASHENG HONG (Fellow, IEEE) received the D.Phil. degree in engineering science from the University of Oxford, Oxford, U.K., in 1994.

He then, joined the University of Birmingham, Birmingham, U.K., until 2001, when he moved up to Edinburgh, U.K., to join Heriot-Watt University, Edinburgh, where he is currently a Professor and leading a team for research into advanced radio frequency (RF)/microwave device technologies. He has authored or coauthored over 200 journal articles and conference papers in this field and has published four relevant books: *Microstrip Filters for RF/Microwave Applications* (Wiley, first edition, 2001, and second edition, 2011); *RF and Microwave Coupled-Line Circuits* (Artech House, second edition, 2007); *Balanced Microwave Filters* (Wiley, 2018); and *Advances in Planar Filters Design* (IET, 2019).

Dr. Hong is a member of the IEEE MTT Technical Committee, the Subject Editor (Microwave) of *Electronics Letters*, and an Associate Editor of *IET Microwaves, Antennas and Propagation*.